Formation of super-Alfvénic electron jets during laser-driven magnetic reconnection at the Shenguang-II facility: particle-in-cell simulations

2014 New J. Phys. 16 083021

(http://iopscience.iop.org/1367-2630/16/8/083021)

New Journal of Physics
The open access journal at the forefront of physics
Deutsche Physikalische Gesellschaft DPG | IOP Institute of Physics

Formation of super-Alfvénic electron jets during laser-driven magnetic reconnection at the Shenguang-II facility: particle-in-cell simulations

San Lu[1], Quanming Lu[1], Can Huang[1], Quanli Dong[2], Jianqiang Zhu[3], Zhengming Sheng[4,5], Shui Wang[1] and Jie Zhang[4]

[1] CAS Key Lab of Geospace Environment, University of Science and Technology of China, Hefei 230026, People's Republic of China
[2] School of Physics and Optoelectronic Engineering, Ludong University, Yantai 264025, People's Republic of China
[3] CAS Key Laboratory for High Power Laser Physics, Chinese Academy of Sciences, Shanghai 201800, People's Republic of China
[4] MoE Key Laboratory for Laser Plasmas and Department of Physics, Shanghai Jiao Tong University, Shanghai 200240, People's Republic of China
[5] SUPA, Department of Physics, University of Strathclyde, Glasgow G4 ONG, UK
E-mail: qmlu@ustc.edu.cn

Received 16 April 2014, revised 30 May 2014
Accepted for publication 18 June 2014
Published 8 August 2014

New Journal of Physics **16** (2014) 083021

doi:10.1088/1367-2630/16/8/083021

Abstract

Magnetic reconnection experiments in high-energy-density (HED) laser-produced plasmas have recently been conducted at the Shenguang-II (SG-II) facility. Two plasma bubbles and a 'frozen-in' magnetic field are generated by irradiating an Al foil using two laser beams. As the two bubbles with opposing magnetic fields expand and squeeze each other, magnetic reconnection occurs. In the experiments, three well-collimated high-speed electron jets are observed in the fanlike outflow region of the laser-driven magnetic reconnection. Based on two-dimensional (2D) particle-in-cell (PIC) simulations, we demonstrate that the three electron jets in the outflow region of laser-driven magnetic reconnection are super-Alfvénic, and their formation mechanism is also revealed in this paper. The two super-Alfvénic jets at the edge are formed by the outflow electrons, which move along magnetic field lines after they are accelerated in the vicinity of the X-line by the reconnection electric field. The super-Alfvénic jet at

the center is formed by the electrons that come from the outside of the plasma bubbles. These electrons are reflected by the magnetic field in the pileup region and are meanwhile accelerated by the resulting electric field.

Keywords: magnetic reconnection, laser-produced plasmas, electron jet

1. Introduction

Magnetic reconnection is a fundamental plasma process that provides a mechanism of efficient and fast conversion of magnetic energy to plasma kinetic and thermal energy [1–3]. The topological structures of magnetic field lines are also changed during the reconnection process. Magnetic reconnection is believed to be the driving mechanism of many explosive phenomena in space and laboratory plasmas, such as flares in the solar atmosphere [4, 5], flux transfer events (FTEs) [6–8], substorms [9, 10] in the Earth's magnetosphere and disruptions in laboratory fusion experiments [11]. Magnetic reconnection is also found to occur in the magnetotail of non-magnetized planets [12, 13].

The first series of dedicated laboratory experiments has been performed to investigate the process of magnetic reconnection. This includes the magnetic reconnection experiment (MRX) [14], Versatile Toroidal Facility (VTF) [15] and Todai Spheromark-3/4 (TS-3/4) [16, 17]. Besides these experiments, the high-energy-density (HED) laser-plasma experiment has recently been found to provide a new platform for the study of magnetic reconnection. Plasma bubbles are created by focusing HED laser beams on a planar foil target, and an azimuthal magnetic field is self-generated through noncollinear electron density and temperature gradients ($\nabla n_e \times \nabla T_e$) around the laser spot [18]. The magnetic field is approximately 'frozen' in the plasma bubbles. As the bubbles with the opposing magnetic field expand and eventually encounter each other, magnetic reconnection occurs in the current sheet formed between the plasma bubbles. The first experimental measurement of the magnetic field and plasma dynamics in such a geometry was carried out by Nilson *et al* [19] and Li *et al* [20]. In their experiments, highly collimated bidirectional plasma jets and topological changes of the magnetic field were observed, which indicate the occurrence of magnetic reconnection. After the experimental observations of laser-driven magnetic reconnection, two-dimensional (2D) particle-in-cell (PIC) simulations were performed by Fox *et al* [21, 22]. to study magnetic reconnection between two laser-produced plasma bubbles with parameters and geometry based on the experiments. It was found that the reconnection rate, which is faster than the prediction by the Hall reconnection model in such a strongly driven system, can be explained by substantial upstream flux-pileup effects, which enhance the relevant magnetic field intensity in the current sheet.

The generation of energetic electrons is considered to be an important signature in magnetic reconnection. In solar flare observations, it has been estimated that up to 50% of the released energy is taken by energetic electrons [23, 24]. In the Earth's magnetotail, energetic electrons up to several hundreds of keV have been detected in the vicinity of the reconnection site [25–29]. The acceleration mechanism of energetic electrons has been studied in the Harris current sheet model—the electrons move towards the vicinity of the X-line along the separatrices, where they are accelerated by the reconnection electric field, and then are directed away from the X-line along the magnetic field lines just inside the separatrices [30–33]. The

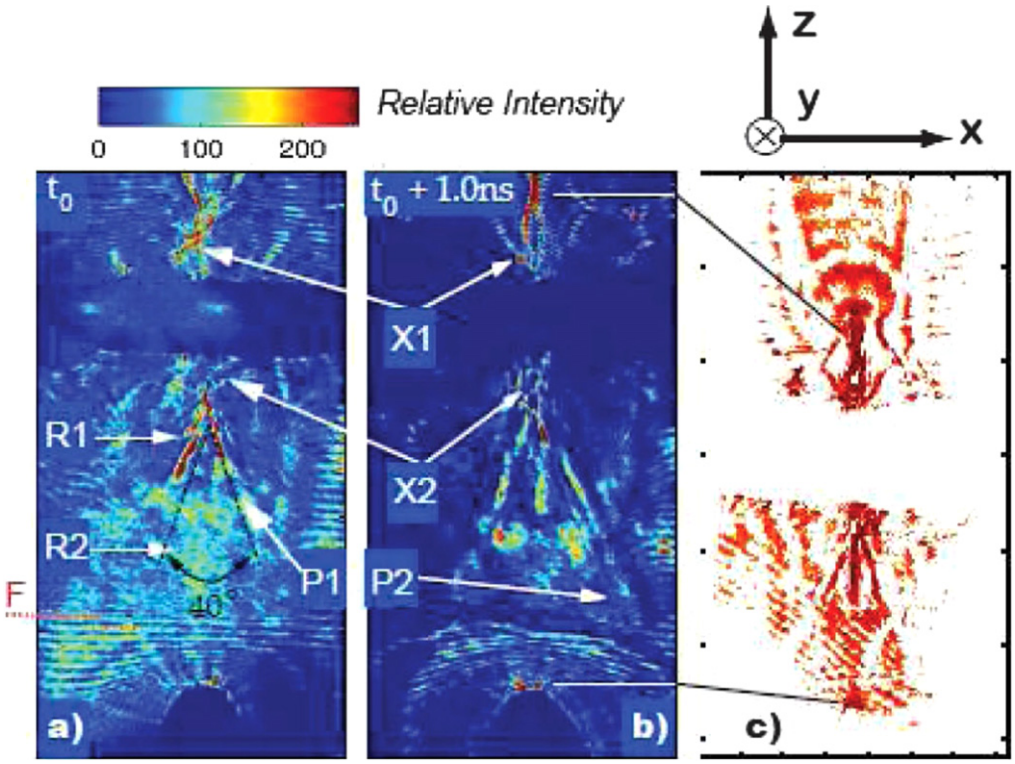

Figure 1. Interferometric image at (a) $t = t_0$ and (b) $t = t_0 + 1$ns, where t_0 is set at the half maximum of the laser pulse tail. The electron diffusion region is between X1 and X2. R1 points to a fanlike outflow region, and R2 points to a relatively calm and uniform plasma region. P1 and P2 mark the location of a front of the expanding fanlike region at the two times. (c) A linearly polarized self-emission image of the plasma. The details of the experiment can be found in Dong *et al* [39].

reconnection outflow electron jets are considered to be super-Alfvénic [34–37], which has been verified during magnetic reconnection observed in the magnetotail [38].

Recently, the laser-driven magnetic reconnection experiment has also been conducted at the Shenguang-II (SG-II) laser facility [39]. Figures 1(a) and (b) show the interferometric images of the laser-generated plasma at $t = t_0$ and $t = t_0 + 1$ns, respectively, where t_0 is set at the half maximum of the laser-pulse tail. Figure 1(c) shows the profile of the linearly polarized self-emission from the plasma. The region between X1 and X2 is the electron diffusion region. The details of the experiment can be found in Dong *et al* [39]. From the figure, a plasmoid and three well-collimated high-speed electron jets are shown during the reconnection. The generation mechanism of the plasmoid during reconnection in HED laser-produced plasmas has been investigated in Lu *et al* [40]. The three well-collimated high-speed electron jets are formed in the fanlike outflow region. The energy of the energetic electrons in the three jets can reach MeVs, and their spectrum exhibits a power-law scaling at the high-energy tail for electrons up to 2 MeV. In this paper, with 2D PIC simulations, the formation mechanism of the three electron jets is investigated. The simulation parameters and geometry are based on the reported SG-II experiments.

The outline of the paper is as follows. In section 2, the simulation model is described, section 3 presents the simulation results, and section 4 gives the conclusions and discussion.

2. Simulation model

In the 2D PIC simulation model, the electromagnetic field is defined on the grids and updated by solving Maxwell's equations with a full explicit algorithm, and the ions and electrons are advanced in the electromagnetic field. The initial configuration of the simulation system is two expanding semicircular plasma bubbles in the (x, z) plane, which is in accord with the previous PIC simulations by Fox *et al* [21, 22]. The computation is carried out in a rectangular domain in the (x, z) plane with the dimensions $[-L_x, L_x] \times [-L_z, L_z]$. The two semicircular bubbles are centered at $(0, -L_z)$ and $(0, L_z)$, respectively. The radius vectors of the bubbles are defined from the center of each bubble, which can be expressed as $\mathbf{r}^{(1)} = (x, z + L_z)$ and $\mathbf{r}^{(2)} = (x, z - L_z)$. The initial number density is $n_b + n^{(1)} + n^{(2)}$, where n_b is a background density, and $n^{(i)}$ (i = 1, 2) is

$$n^{(i)} = \begin{cases} (n_0 - n_b)\cos^2\left(\dfrac{\pi r^{(i)}}{2L_n}\right) & \text{if } r^{(i)} < L_n, \\ 0 & \text{otherwise,} \end{cases} \tag{1}$$

where L_n is the initial scale of the bubbles and n_0 is the peak bubble density. Initially, the bubbles expand radially, and the velocity is expressed as the sum of the following fields

$$\mathbf{V}^{(i)} = \begin{cases} V_0 \sin\left(\dfrac{\pi r^{(i)}}{L_n}\right)\hat{\mathbf{r}}^{(i)} & \text{if } r^{(i)} < L_n, \\ 0 & \text{otherwise,} \end{cases} \tag{2}$$

where V_0 is the initial expanding speed of the two plasma bubbles. The magnetic field is initialized as the sum of two toroidal ribbons, with

$$\mathbf{B}^{(i)} = \begin{cases} B_0 \sin\left(\dfrac{\pi\left(L_n - r^{(i)}\right)}{2L_B}\right)\hat{\mathbf{r}}^{(i)} \times \hat{\mathbf{y}} & \text{if } r^{(i)} \in \left[L_n - 2L_B, L_n\right], \\ 0 & \text{otherwise,} \end{cases} \tag{3}$$

where B_0 is the initial strength of the magnetic field, and L_B is the half-width of the magnetic ribbons. In order to be consistent with the plasma flow, an initial electric field $\mathbf{E} = -\mathbf{V} \times \mathbf{B}$ is added, while the initial out-of-plane current density is determined by Faraday's law.

The simulation parameters are chosen based on the reported or estimated SG-II experimental parameters, which are listed in table 1 [39]. The measured electron density near the X-line is $\sim 5 \times 10^{19}\ \mathrm{cm}^{-3}$, which is about one tenth of the peak electron density. Therefore, the peak electron density is about $5 \times 10^{20}\ \mathrm{cm}^{-3}$. The estimated average ionic charge is about $Z \sim 10$, and thus the peak ion density is about $5 \times 10^{19}\ \mathrm{cm}^{-3}$. The ion inertial length based on the peak ion density is about $d_i = c/\omega_{pi} = 16.8\ \mu\mathrm{m}$. The measured plasma bubble radius is about $L_n = 200\ \mu\mathrm{m}$, and the width of the magnetic ribbons, $2L_B$, is about $80\ \mu\mathrm{m}$. In our PIC simulations, we choose $L_n = 12d_i$ and $L_B = 2d_i$. The self-generated magnetic field in laser-plasma interaction is at the order of mega-gauss (MG) [19, 20, 41, 42]. In the SG-II experiments, the magnetic field is estimated to be around 3.75 MG after the bubbles have been strongly squeezed. Therefore, it is several times larger than the initial magnetic field. So in the simulations, we choose the initial magnetic field $B_0 = 2$ MG. The mass ratio m_i/m_e is set to be

Table 1. SG-II experimental parameters [39].

Parameter		Reported or estimated values
Ions		Al
Average ionic charge	Z	~10
Peak electron density	n_{e0}	$\sim 5 \times 10^{20}$ cm^{-3}
Peak ion density	n_{i0}	$\sim 5 \times 10^{19}$ cm^{-3}
Plasma bubble scale	L_n	200 μm
Width of magnetic ribbon	$2L_B$	80 μm
Temperature	T_e, T_i	570 eV
Magnetic field	B_0	2 MG
Estimated inflow speed	V_0	5.4×10^5 m s^{-1}
Ion inertial length	$d_i = c/\omega_{pi}$	16.8 μm
Alfvén speed	v_A	1.2×10^5 m s^{-1}
Electron beta	β_e	2.9
Sound speed	$C_s = \left(\gamma Z T_e/m_i\right)^{1/2}$	1.8×10^5 m s^{-1}
Electron mean-free-path	$\lambda_{mfp,e}$	600 μm

100 and the light speed c is $75v_A$ (where v_A is the Alfvén speed based on B_0 and n_{i0}). We choose $n_b = 0.2n_0$, and uniform initial ion and electron temperatures are adopted for simplicity: $T_{i0} = T_{e0} = 0.025m_e c^2$. The initial distribution functions for the ions and electrons are Maxwellian, with the bulk velocities in the radial direction (described by equation (2)) and drift velocities in the y direction and which supply the out-of-plane current density. The initial expansion speed of the plasma bubbles is $V_0 = 3C_s$, where $C_s = \left(\gamma Z T_e/m_i\right)^{1/2}$ is the sound speed. We set $L_x = 25.6c/\omega_{pi}$ and $L_z = 12.8c/\omega_{pi}$, and the number of grid points is $N_x \times N_z = 1024 \times 512$ with a spatial resolution of $\Delta x = \Delta z = 0.05c/\omega_{pi}$. The time step is $\Omega_i t = 0.0001$ ($\Omega_i = eB_0/m_i$ is the ion gyrofrequency). More than 2×10^8 particles per species are employed to simulate the plasmas. In the simulations, periodic boundary conditions are used along both the x and z directions.

3. Simulation results

Figure 2 shows the magnetic field B/B_0 and out-of-plane current density $j_y/(en_0 v_A)$ at $\Omega_i t =$ (a) 0, (b) 1.1, (c) 2 and (d) 2.75, respectively. The magnetic field lines are also plotted in the figure. The plasma bubbles squeeze each other strongly because of the supersonic expansion. Therefore, the magnetic flux is piled up in the inflow region before it is reconnected. At $\Omega_i t = 1.1$, just before the reconnection begins, the upstream magnetic field is strongly enhanced, with a maximum about $3B_0$. The pileup of the upstream magnetic flux is considered to be the key to understanding the faster rate of reconnection observed in laser-produced plasma bubbles than the prediction by the Hall reconnection model [21, 22, 40]. With the pileup of the upstream magnetic flux, a long and thin current sheet is formed between the two plasma bubbles. The maximum of the out-of-plane current density is about $6en_0 v_A$, and the length and half-width of the current sheet are $14.05c/\omega_{pi}$ and $0.675c/\omega_{pi}$, respectively. Here, the length of the current sheet is defined as the length of the region where j_y is larger than zero along $z = 0$, and the

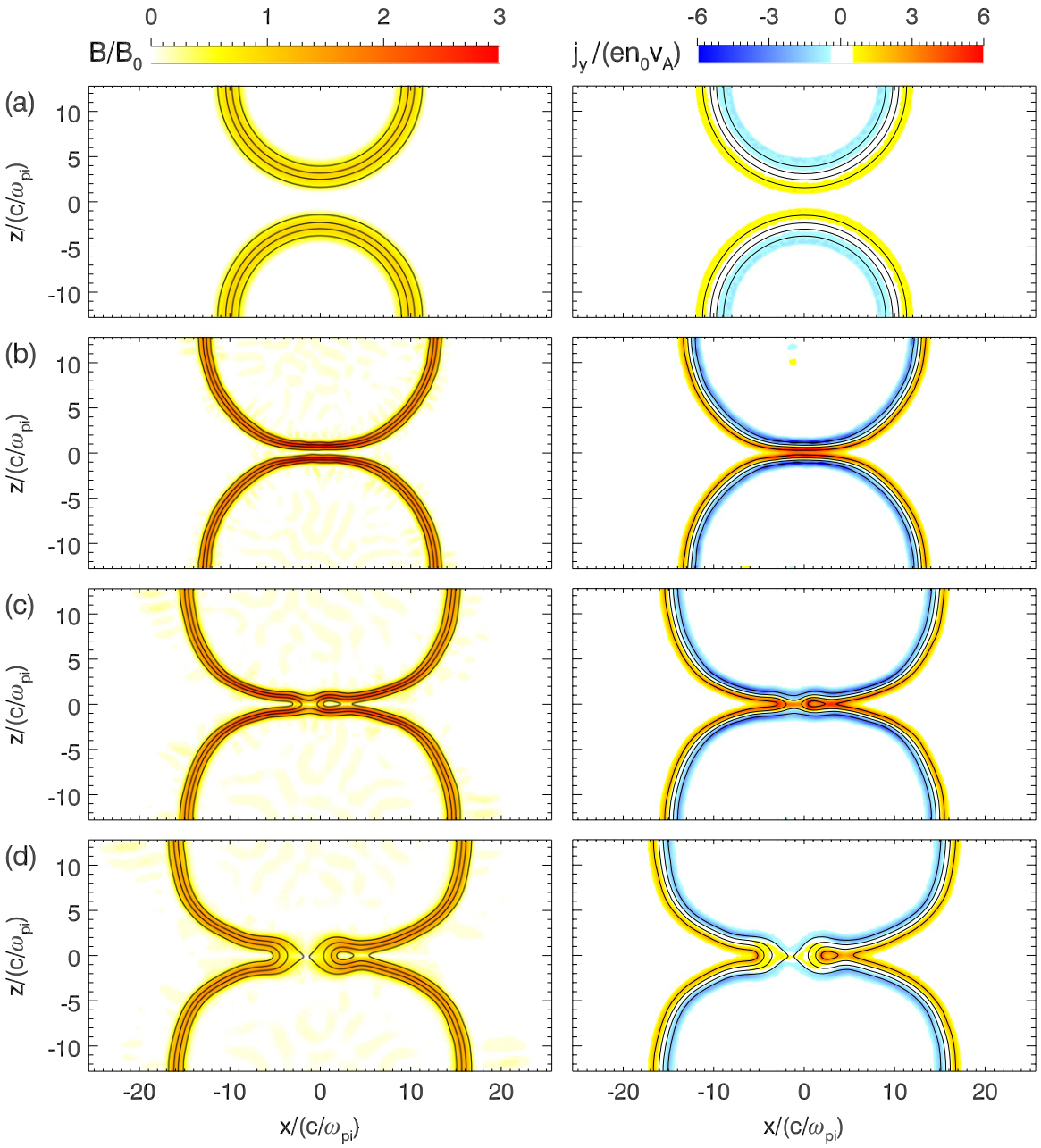

Figure 2. Magnetic field magnitude B/B_0 (left column) and out-of-plane current density $j_y/(en_0v_A)$ (right column) at $\Omega_i t =$ (a) 0, (b) 1.1, (c) 2 and (d) 2.75. The black lines denote the magnetic field lines in the (x, z) plane.

width of the current sheet is defined as the distance between the positive and negative peaks of B_x along $x = 0$. Based on the linear theory of the tearing mode instability [43, 44], the maximum growth rate occurs around $k\delta = 2\pi M\delta/L = 0.55$, where $M = 1, 2, 3, \ldots$. Therefore, the most unstable tearing mode is $M = 2$ ($k\delta \approx 0.6$), which is consistent with the simulation result: at $\Omega_i t = 2$, two reconnection X-lines are generated in the current sheet, and a plasmoid is formed between the two X-lines. The formation of the plasmoid has also been observed in laser-produced plasma reconnection at the SG-II facility [39]. Magnetic reconnection gradually slows

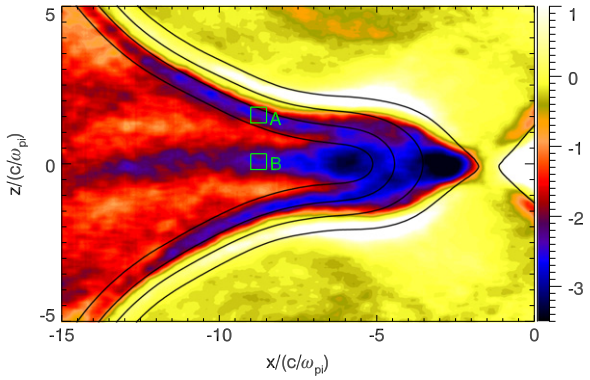

Figure 3. Electron bulk velocity in the x direction V_{ex}/v_A at $\Omega_i t = 2.75$. The black lines represent the magnetic field lines in the (x, z) plane.

down after $\Omega_i t \approx 2$, and the magnetic flux flowing outward begins to pile up in the outflow region. Meanwhile, with the development of magnetic reconnection, the plasmoid grows larger and gradually merges into the outflow region in the right side.

Figure 3 shows the electron bulk velocity along the x direction, V_{ex}/v_A at $\Omega_i t = 2.75$. The magnetic field is weak in the vicinity of the X line, therefore, there forms a magnetic mirror geometry in the electron inflow region. The electrons sense a magnetic mirror force $\mathbf{F} = \mu \nabla B$ when they are injected to the vicinity of the X-line along the magnetic field. The electron inflow speed is about $1.0v_A$. In the fanlike outflow region, three well-collimated super-Alfvénic electron jets, which are directed away from the X-line, are observed. Such a phenomenon has been observed in the SG-II laser-driven magnetic reconnection experiment, which is shown in figures 1(a) and (b). The two jets at the edge flow out along the magnetic field lines just inside the separatrices, and the one at the center is in the middle of the outflow region. The maximum speed of the electron jets is about $4v_A$ ($\approx$480 km s^{-1}), the opening angle of the outflow region is about 40°, and the width of the jets is about one ion inertial length. In the SG-II experiment, the speed of the electron jets is about 600km/s, the opening angle is 35°−40°, and the width is $0.75c/\omega_{pi} - 1c/\omega_{pi}$ [39], which shows a good consistency between the simulation and experiment. Note that at $\Omega_i t = 2.75$, the upstream magnetic field is about $0.4B_0$, and the density in the X-line is about $0.3n_0$. Therefore, the instantaneous Alfvén speed $v_A^* \approx 0.73v_A$, so the maximum speed of the electron jets is about $5.5v_A^*$. Figure 4 shows the electron number density n_e/n_0 and energy spectrum in the outflow region $x \in [-8, -7]\, c/\omega_{pi}$, $z \in [-1.5, 1.5]\, c/\omega_{pi}$ (within the red rectangle in figure 4(a)) at $\Omega_i t = 2.75$. It shows that the electron density in the outflow region is relatively higher than that in the inflow region. The electron energy spectrum in the jets obeys a power-law scaling at the high-energy tail, and the power-law index is −6.76, which is also consistent with the SG-II experimental results.

In order to reveal the formation mechanism of the super-Alfvénic electron jets in the outflow region, we 'tag' these electrons in the super-Alfvénic jets at $\Omega_i t = 2.75$. Then the simulation is re-run to trace the position and energy of each tagged electron. Figure 5 presents the spatial and energy distributions of the tagged electrons at four different times: $\Omega_i t =$ (a) 0, (b) 1.8, (c) 2.6 and (d) 2.75. All these tagged electrons move to the region 'A' (marked in figure 3) and contribute to the upper super-Alfvénic electron jet at $\Omega_i t = 2.75$. Initially, most of these electrons are located in the flux tube at the edge of the two plasma bubbles. With the proceeding of magnetic reconnection, these electrons are injected into the vicinity of the X-line

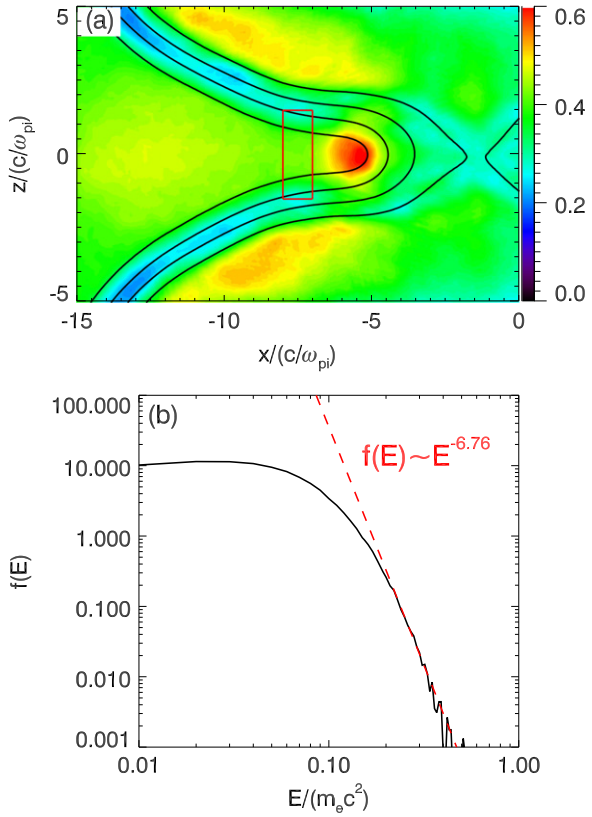

Figure 4. (a) Electron number density n_e/n_0 and (b) energy spectrum in the outflow region $x \in [-8, -7]c/\omega_{pi}$, $z \in [-1.5,1.5]c/\omega_{pi}$ (within the red rectangle in figure 4(a)) at $\Omega_i t = 2.75$. The black lines represent the magnetic field lines in the (x, z) plane.

and accelerated by the reconnection electric field. Then, the accelerated electrons are directed away from the X-line along the magnetic field lines just inside the separatrix. Therefore, two super-Alfvénic electron jets are eventually formed at the edge of the fanlike outflow region. The increase of the colour-coded energy shows that the electrons are accelerated during this process, especially after magnetic reconnection begins. At $\Omega_i t = 0$, the energy of the tagged electrons is around the initial temperature $0.025\ m_e c^2$. At $\Omega_i t = 2.6$, some of the tagged electrons can be accelerated to $0.3\ m_e c^2$ or even higher energies.

In order to further clarify the formation mechanism of the two super-Alfvénic electron jets at the edge of the fanlike outflow region, figure 6 shows the trajectory of a typical electron from the upper jet. In the figure, the trajectory is divided into three segments: (a) $1.6 \leqslant \Omega_i t \leqslant 2$, (b) $2 \leqslant \Omega_i t \leqslant 2.25$ and (c) $2.25 \leqslant \Omega_i t \leqslant 2.65$. The contours present the out-of-plane electric field $E_y/\left(v_A B_0\right)$ and magnetic field lines at $\Omega_i t =$ (a) 1.8, (b) 2.15 and (c) 2.45. The time evolution of the electron energy $E_e/\left(m_e c^2\right)$ is shown in figure 6(d). During $1.6 \leqslant \Omega_i t \leqslant 2$, the electron moves towards the X-line due to the effect of the magnetic mirror, thus electron energy is nearly unchanged in the segment. From $\Omega_i t = 2$ to $\Omega_i t = 2.25$, the electron is accelerated by the reconnection electric field in the vicinity of the X-line. The accelerated electron then leaves the X-line region along the magnetic field lines.

Figure 7 presents the tracing results of the tagged electrons in the center super-Alfvénic electron jet, with (a), (b), (c) and (d) showing spatial and energy distributions of the tagged

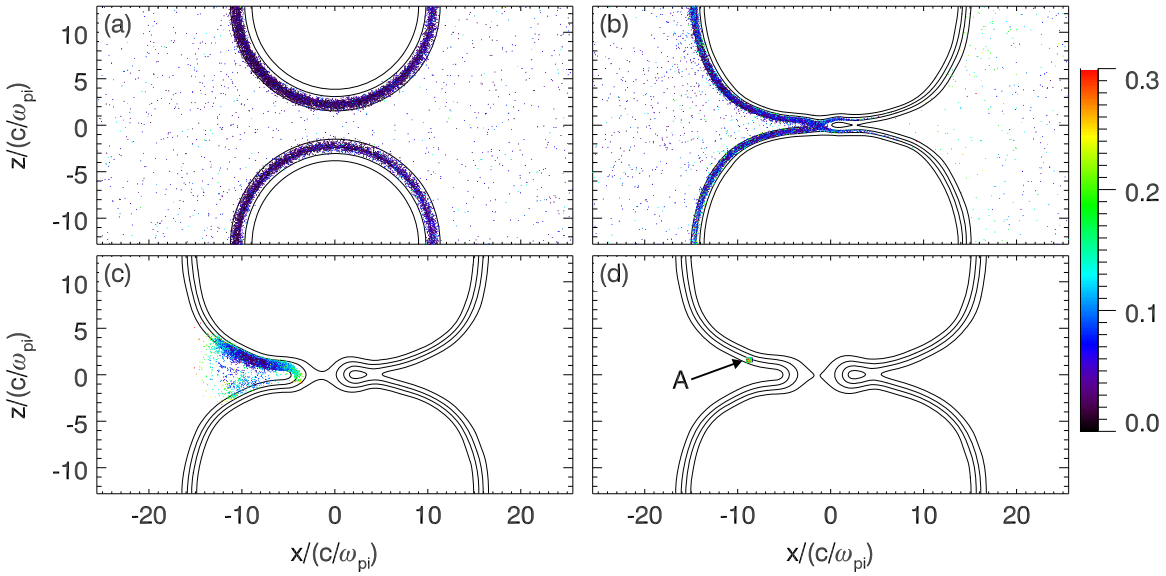

Figure 5. The distribution of the 'tagged' electrons at the upper outflow jet (within the rectangle denoted by 'A' in figure 3). Here (a), (b), (c) and (d) represent the spatial distributions of the 'tagged' electrons at $\Omega_i t = 0$, 1.8, 2.6 and 2.75, respectively. The colour represents the energy of the 'tagged' electrons $E_e/(m_e c^2)$, and the black lines represent the magnetic field lines.

electrons at $\Omega_i t = 0$, 1.8, 2.6, and 2.75, respectively. All these tagged electrons move to the region 'B' (marked in figure 3) and contribute to the center outflow jet at $\Omega_i t = 2.75$. These electrons are initially located in the region outside of the plasma bubbles with an averaged energy of about 0.025 $m_e c^2$. With the development of magnetic reconnection, the magnetic flux is piled up in the outflow region. The magnetic field lines move outward quickly due to the push of the electrons accelerated in the vicinity of the X-line. The electrons outside of the plasma bubbles are then reflected by the magnetic field in the pileup region, and meanwhile they are accelerated by the resulting electric field E_y. At $\Omega_i t = 2.6$, some of the tagged electrons can be accelerated to 0.3 $m_e c^2$, and the highest energy can reach 0.54 $m_e c^2$. Thus the center super-Alfvénic electron jet in the middle of the outflow region is formed.

Figure 8 shows the trajectory and energy evolution of a typical electron from the center super-Alfvénic jet. The trajectory is also divided into three segments: (a) $2.4 \leqslant \Omega_i t \leqslant 2.57$, (b) $2.57 \leqslant \Omega_i t \leqslant 2.64$ and (c) $2.64 \leqslant \Omega_i t \leqslant 2.75$. The contours present the out-of-plane electric field $E_y/\left(v_A B_0\right)$ and magnetic field lines at $\Omega_i t =$ (a) 2.5, (b) 2.6 and (c) 2.7. The time evolution of the electron energy $E_e/\left(m_e c^2\right)$ is shown in figure 8(d). During $2.4 \leqslant \Omega_i t \leqslant 2.57$, the electrons move towards the pileup region with a relatively low speed, and the energy is nearly unchanged in the segment. During $2.57 \leqslant \Omega_i t \leqslant 2.64$, the electron is reflected by the magnetic ribbon, but the energy is almost unchanged. The magnetic field in the background region is very weak, so there is a sharp boundary between the background region and the pileup region. From $\Omega_i t = 2.64$, as the electron begins to penetrate through the boundary into the pileup region, it senses a $\mathbf{v}_e \times \mathbf{B}$ Lorentz force, which causes it to gyrate about half an orbit. Meanwhile, the electron is accelerated in the y direction by the electric field E_y. After this process, at about $\Omega_i t = 2.67$, the electron leaves the pileup region and moves back into the background region

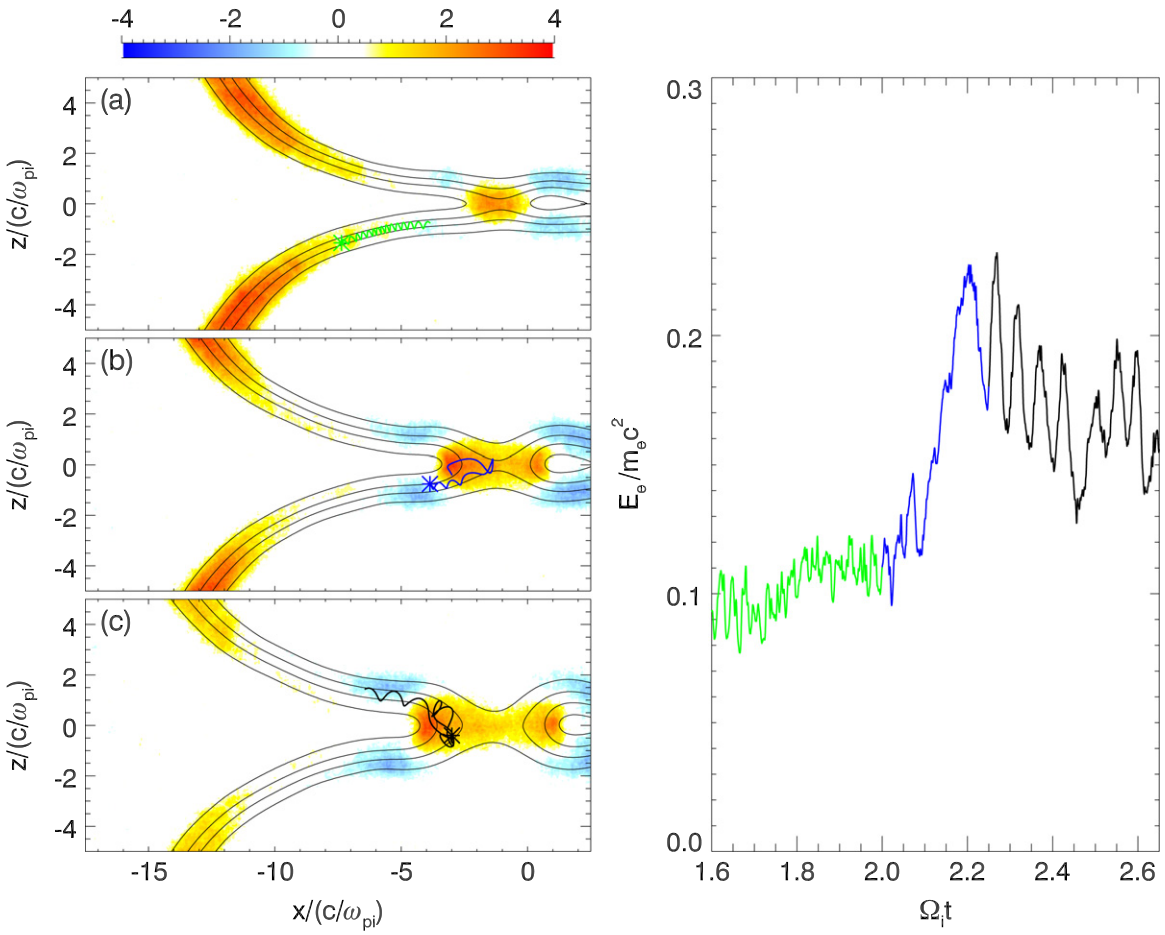

Figure 6. The trajectory (a)–(c) and energy evolution (d) of a typical electron from the upper super-Alfvénic jet. The trajectory is divided into three segments: (a) $1.6 \leqslant \Omega_i t \leqslant 2$ (green), (b) $2 \leqslant \Omega_i t \leqslant 2.25$ (blue) and (c) $2.25 \leqslant \Omega_i t \leqslant 2.65$ (black). The start position of the particle in each segment is marked with an asterisk. The contours present the out-of-plane electric field $E_y/(v_A B_0)$ and magnetic field lines at $\Omega_i t =$ (a) 1.8, (b) 2.15 and (c) 2.45.

along the $-x$ direction with larger energy. The acceleration mechanism is similar to the formation of the energetic particles reflected by shocks [45, 46].

4. Conclusions and discussion

Magnetic reconnection experiments between laser-produced plasma bubbles that provide a new experimental platform for the study of magnetic reconnection have recently been conducted [19, 20]. Dong *et al* [39] observed three well-collimated high-speed jets in the fanlike outflow region during the laser-driven magnetic reconnection at the SG-II facility. In this paper, with 2D PIC simulations, we demonstrate that the three electron jets are super-Alfvénic, and their origins are different. The two electron jets at the edge are formed by the energetic electrons that are accelerated in the vicinity of the X-line and directed away along magnetic field lines just inside the separatrices. The electron jet at the center is formed by the energetic electrons that come

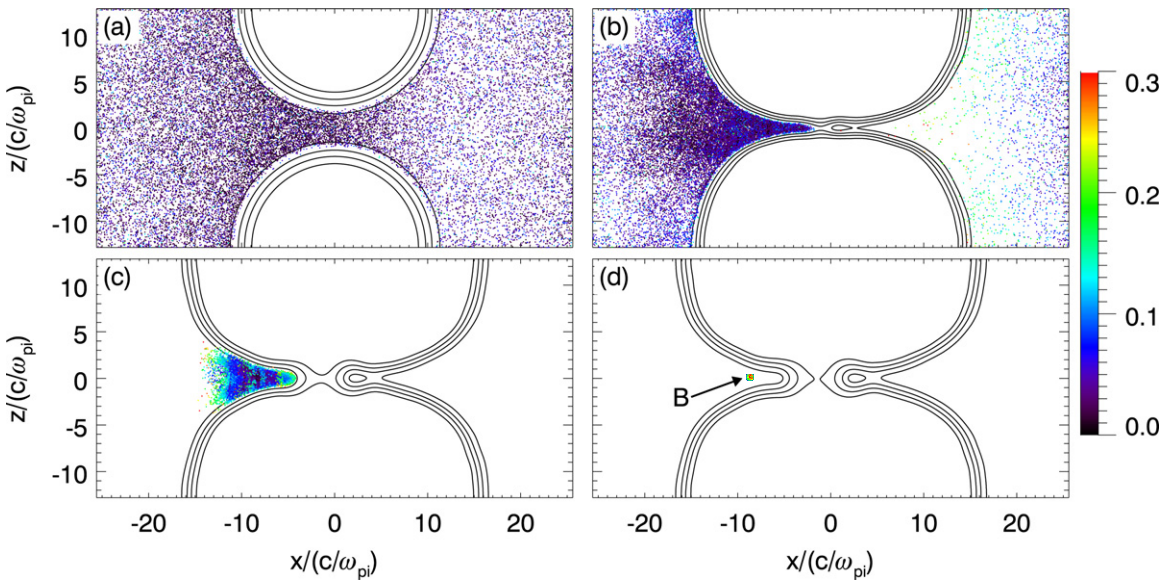

Figure 7. The distribution of the 'tagged' electrons at the center outflow jet (within the rectangle denoted by 'B' in figure 3). Here (a), (b), (c) and (d) represent the spatial distributions of the 'tagged' electrons at $\Omega_i t = 0$, 1.8, 2.6 and 2.75, respectively. The colour represents the energy of the 'tagged' electrons $E_e/(m_e c^2)$, and the black lines represent the magnetic field lines.

from the region outside of the plasma bubbles. They are reflected by the magnetic field in the pileup region. During the reflection, the electrons are accelerated by the resulting electric field E_y.

The formation mechanism of the two electron jets at the edge is analogous to that of magnetic reconnection in a Harris current sheet [30–33], and such super-Alfvénic jets have also been observed by Cluster during magnetic reconnection in the magnetosheath region downstream of the Earth's bow shock [38]. However, during the laser-driven magnetic reconnection, the electrons outside the plasma bubbles may be reflected by the fast moving magnetic field and then accelerated in the pileup region of the outflow region, thus the third super-Alfvénic electron jet can be formed at the center of the outflow region. The existence of such a super-Alfvénic electron jet in the outflow region is evidence that the magnetic field lines also move outward with a super-Alfvénic speed during the reconnection; therefore, it is one of the key signatures of fast magnetic reconnection.

In Harris current sheet geometry, there is also a central electron outflow jet. However, it is within the electron diffusion region, and the electrons in the jet are originally from the upstream region. A similar jet also exists in laser-driven reconnection geometry (see the region $x \sim -3c/\omega_{pi}$ in figure 3). However, in this paper, we focus on the high-speed electron jet in the fanlike outflow region.

Coulomb collisions may play some role in the laser-driven reconnection experiments. In the SG-II experiment [39], the electron number density in the vicinity of the X-line is $n_e \approx 5 \times 10^{25}\ \mathrm{m}^{-3}$, and the electron temperature is $T_e \approx 570$ eV. Therefore, the electron mean-free-path is $\lambda_{mfp,e} \approx 600\ \mu$m [47], while the characteristic spatial scale of the SG-II reconnection is $\sim 100\ \mu$m. Given this, the effect of Coulomb collisions is negligible in the SG-II experiment and will not change the conclusions in this paper. Actually, Fox *et al* [22] have demonstrated

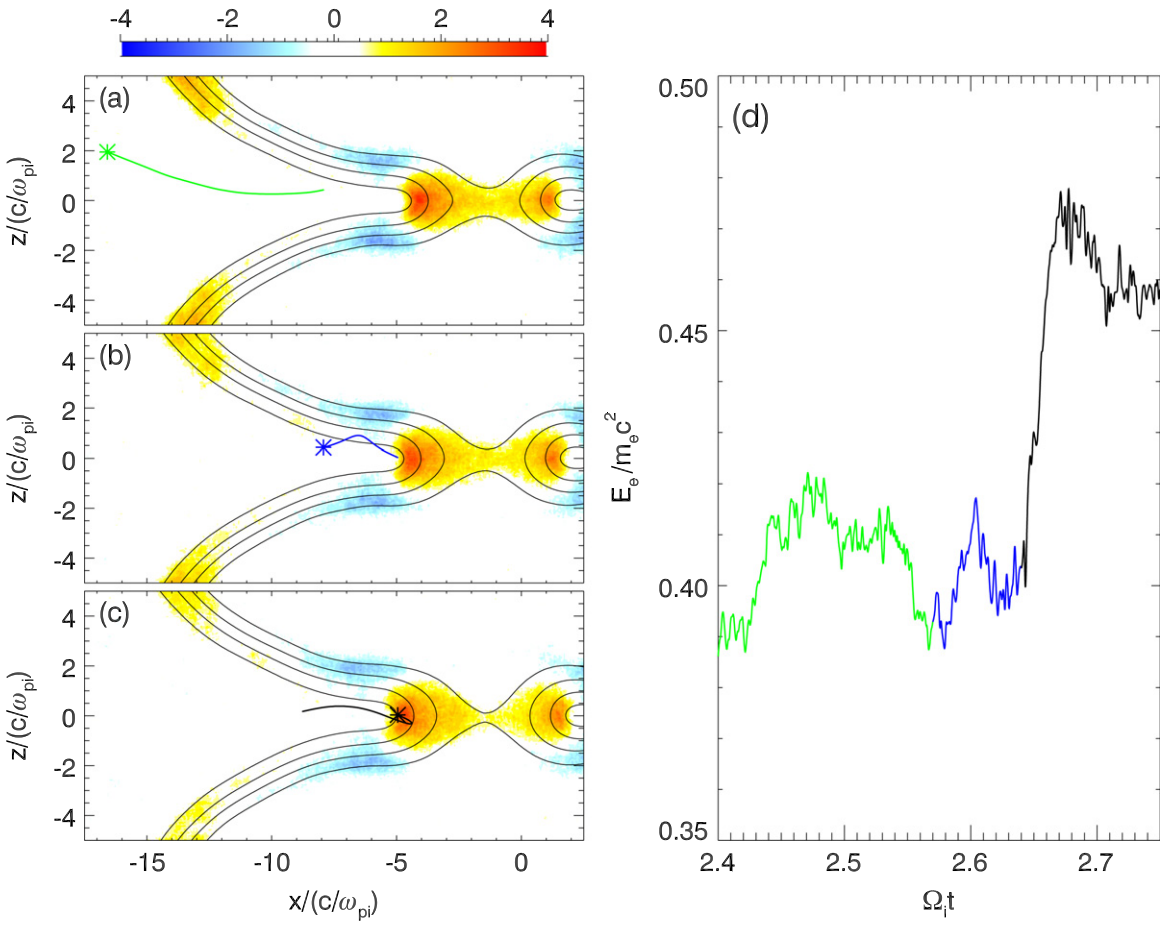

Figure 8. The trajectory (a)–(c) and energy evolution (d) of a typical electron from the super-Alfvénic jet at the center. The trajectory is divided into three segments: (a) $2.4 \leqslant \Omega_i t \leqslant 2.57$ (green), (b) $2.57 \leqslant \Omega_i t \leqslant 2.64$ (blue) and (c) $2.64 \leqslant \Omega_i t \leqslant 2.75$ (black). The start position of the particle in each segment is marked with an asterisk. The contours present the out-of-plane electric field $E_y/\left(v_A B_0\right)$ and magnetic field lines at $\Omega_i t =$ (a) 2.5, (b) 2.6 and (c) 2.7.

that the collisions may slow down the reconnection process to some extent (although it is still very fast), while the evolution of density and upstream magnetic field is not changed.

Acknowledgements

This work was supported by 973 Program (2013CBA01503, 2012CB825602), the National Science Foundation of China (NSFC) under grants 41331067, 41274144, 41174124, 41121003 and CAS Key Research Program KZZD-EW-01.

References

[1] Biskamp D 2000 *Magnetic Reconnection in Plasmas* (Cambridge: Cambridge University Press)

[2] Birn J and Priest E R 2007 *Reconnection of Magnetic Fields: Magnetohydrodynamics and Collisionless Theory and Observations* (Cambridge: Cambridge University Press)
[3] Yamada M, Kulsrud R and Ji H T 2010 *Rev. Mod. Phys.* **82** 603
[4] Giovanelli R G 1946 *Nature* **158** 81
[5] Tsuneta S, Hara H, Shimizu T, Acton L W, Strong K T, Hudson H S and Ogawara Y 1992 *Publ. Astron. Soc. Jpn.* **44** L63
[6] Russell C T and Elphic R C 1978 *Space Sci. Rev.* **22** 681
[7] Lee L C and Fu Z F 1985 *Geophys. Res. Lett.* **12** 105
[8] Hasegawa H *et al* 2010 *Geophys. Res. Lett.* **37** L16101
[9] Baker D N, Pulkkinen T I, Angelopoulos V, Baumjohann W and McPherron R L 1996 *J. Geophys. Res.* **101** 12975
[10] Angelopoulos V *et al* 2008 *Science* **321** 931
[11] Wesson J 1997 *Tokomaks* (New York: Oxford University Press)
[12] Eastwood J P, Brain D A, Halekas J S, Drake J F, Phan T D, Øieroset M, Mitchell D L, Lin R P and Acuna M 2008 *Geophys. Res. Lett.* **35** L02106
[13] Zhang T. L. *et al* 2012 *Science* **336** 567
[14] Yamada M, Ji H T, Hsu S, Carter T, Kulsrud R, Bretz N, Jobes F, Ono Y and Perkins F 1997 *Phys. Plasmas* **4** 1936
[15] Egedal J, Fasoli A, Porkolab M and Tarkowski D 2000 *Rev. Sci. Instrum.* **71** 3351
[16] Yamada M, Ono Y, Hayakawa A, Katsurai M and Perkins F 1990 *Phys. Rev. Lett.* **65** 721
[17] Ono Y, Morita A, Katsurai M and Yamada M 1993 *Phys. Fluids* B **5** 3691
[18] Stamper J A, McLean E A and Ripin B H 1978 *Phys. Rev. Lett.* **40** 1177
[19] Nilson P M *et al* 2006 *Phys. Rev. Lett.* **97** 255001
[20] Li C K, Seguin F H, Frenje J A, Rygg J R, Petrasso R D, Town R P J, Landen O L, Knauer J P and Smalyuk V A 2007 *Phys. Rev. Lett.* **99** 055001
[21] Fox W, Bhattacharjee A and Germaschewski K 2011 *Phys. Rev. Lett.* **106** 215003
[22] Fox W, Bhattacharjee A and Germaschewski K 2012 *Phys. Plasmas* **19** 056309
[23] Lin R P and Hudson H S 1976 *Sol. Phys.* **50** 153
[24] Holman G D, Sui L H, Schwartz R A and Emslie A G 2003 *Astrophys. J.* **595** L97
[25] Øieroset M, Lin R P, Phan T D, Larson D E and Bale S D 2002 *Phys. Rev. Lett.* **89** 195001
[26] Imada S, Nakamura R, Daly P W, Hoshino M, Baumjohann Mühlbachler W S, Balogh A and Reme H 2007 *J. Geophys. Res.* **112** A03202
[27] Chen L J *et al* 2008 *Nat. Phys.* **4** 19
[28] Wang R S, Lu Q M, Du A M and Wang S 2010 *Phys. Rev. Lett.* **104** 175003
[29] Wang R S, Lu Q M, Li X, Huang C and Wang S 2010 *J. Geophys. Res.* **115** A11201
[30] Fu X R, Lu Q M and Wang S 2006 *Phys. Plasmas* **13** 012309
[31] Huang C, Lu Q M and Wang S 2010 *Phys. Plasmas* **17** 072306
[32] Wang R S, Lu Q M, Huang C and Wang S 2010 *J. Geophys. Res.* **115** A01209
[33] Lu Q M, Huang C, Xie J L, Wang R S, Wu M Y, Vaivads A and Wang S 2010 *J. Geophys. Res.* **115** A11208
[34] Daughton W, Scudder J and Karimabadi H 2006 *Phys. Plasmas* **13** 072101
[35] Karimabadi H, Daughton W and Scudder J 2007 *Geophys. Res. Lett.* **34** L13104
[36] Shay M A, Drake J F and Swisdak M 2007 *Phys. Rev. Lett.* **99** 155002
[37] Drake J F, Shay M A and Swisdak M 2008 *Phys. Plasmas* **15** 042306
[38] Phan T D, Drake J F, Shay M A, Mozer F S and Eastwood J P 2007 *Phys. Rev. Lett.* **99** 255002
[39] Dong Q L *et al* 2012 *Phys. Rev. Lett.* **108** 215001
[40] Lu S, Lu Q M, Dong Q L, Huang C, Wang S, Zhu J Q, Sheng Z M and Zhang J 2013 *Phys. Plasmas* **20** 112110
[41] Yates M A, van Hulsteyn D B, Rutkowshi H, Kyrala G and Brackbill J U 1982 *Phys. Rev. Lett.* **49** 1702
[42] Nilson P M *et al* 2008 *Phys. Plasmas* **15** 092701

[43] Pritchett P L, Coroniti F V and Pellat R 1991 *J. Geophys. Res.* **96** 11523
[44] Sitnov M I, Sharma A S, Guzdar P N and Yoon P H 2002 *J. Geophys. Res.* **107** 1256
[45] Yang Z W, Lu Q M, Lembège B and Wang S 2009 *J. Geophys. Res.* **114** A03111
[46] Su Y Q, Lu Q M, Huang C, Wu M Y, Gao X L and Wang S 2012 *J. Geophys. Res.* **117** A08107
[47] Baumjohann W and Treumann R A 1997 *Basic Space Plasma Physics* (London: Imperial College Press)